

Non-Bloch band theory for time-modulated discrete mechanical systems

Kei Matsushima^a, Takayuki Yamada^a

^a*Department of Strategic Studies, Institute of Engineering Innovation, Graduate School of Engineering, The University of Tokyo, 2-11-16 Yayoi, Bunkyo-ku, 113-8656, Tokyo, Japan*

Abstract

This study establishes a non-Bloch band theory for time-modulated discrete mechanical systems. We consider simple mass-spring chains whose stiffness is periodically modulated in time. Using the temporal Floquet theory, the system is characterized by linear algebraic equations in terms of Fourier coefficients. This allows us to employ a standard linear eigenvalue analysis. Unlike non-modulated linear systems, the time modulation makes the coefficient matrix non-Hermitian, which gives rise to, for example, parametric resonance, non-reciprocal wave transmission, and non-Hermitian skin effects. In particular, we study finite-length chains consisting of spatially periodic mass-spring units and show that the standard Bloch band theory is not valid for estimating their eigenvalue distribution. To remedy this, we propose a non-Bloch band theory based on a generalized Brillouin zone. The proposed theory is verified by some numerical experiments.

Keywords: Non-Bloch band theory, Time-modulated system, Non-reciprocal wave propagation, Floquet theory, Non-Hermitian skin effect, Non-Hermitian physics

1. Introduction

It is well known that waves propagating in linear and time-independent media obey reciprocity, i.e., transmission between any two points in space is independent of the propagation direction. In periodic lattices, this implies that Bloch bands are symmetric with respect to the inversion of the Bloch wavevector. Reciprocity holds in a number of classical and quantum systems, e.g., photonics, acoustics, and solid mechanics. Recent studies have revealed

that reciprocity breaks down in nonlinear or time-varying media [1–3]. Broken reciprocity realizes, for example, asymmetric mode conversion [4, 5], unidirectional wave propagation [6–8], and topologically-protected one-way edge modes [9].

To realize non-reciprocity in mechanical systems, the simplest model would be an array of masses and springs whose constants are modulated in time [9–15]. Without using any nonlinear elements, the time modulation allows us to break time-reversal symmetry and reciprocity of the system. Such time-modulated systems are theoretically tractable with the help of the temporal Floquet theory [16–18] and also experimentally feasible using magnets or gyroscopic coupling [7, 9, 12].

When a system is periodic both in space and time, the Bloch–Floquet theory formulates a linear or quadratic eigenvalue problem in terms of angular (quasi)frequency ω for each Bloch wavenumber (wavevector) k . When the eigenvalue problem is written in the form $\mathcal{H}(k)\varphi = \omega\varphi$, the square matrix \mathcal{H} (Bloch Hamiltonian) can be non-Hermitian unlike usual time-independent systems. This means that eigenvalues ω are complex and eigenvectors (eigenmodes) φ generally do not form an orthogonal system. Non-Hermiticity gives rise to unique concepts such as parity-time (PT) symmetry [19, 20], exceptional points [21–23], and non-Hermitian skin effects, which have been intensively studied in the name of non-Hermitian physics [24].

The Bloch band theory with spatial periodicity is a useful tool for estimating the spectral properties of finite-size systems. In usual Hermitian systems, it is well known that Bloch bands represent the spectrum of a lattice (chain) whose size (length) is sufficiently large. The non-Hermiticity defies this conventional knowledge. Due to the presence of non-Hermitian skin effects [25], the standard Bloch (quasi-periodic) condition fails to describe some bulk states. This causes significant differences between the spectrum of finite-size systems with open boundary conditions (OBCs) and purely periodic lattices without boundaries, which can be analyzed from the spectral topology in the complex frequency (energy) plane [26, 27].

The breakdown of the Bloch band theory motivates us to establish a novel framework that is valid for general non-Hermitian systems. A promising approach is the non-Bloch band theory [28, 29] with a generalized Brillouin zone (GBZ) [25, 30]. The non-Bloch band theory allows the wavenumbers (wavevectors) to be complex such that quasi-periodic eigenmodes represent exponentially growing or decaying bulk states. The non-Bloch band theory is validated in some theoretical models (e.g. Hatano–Nelson model [31] and

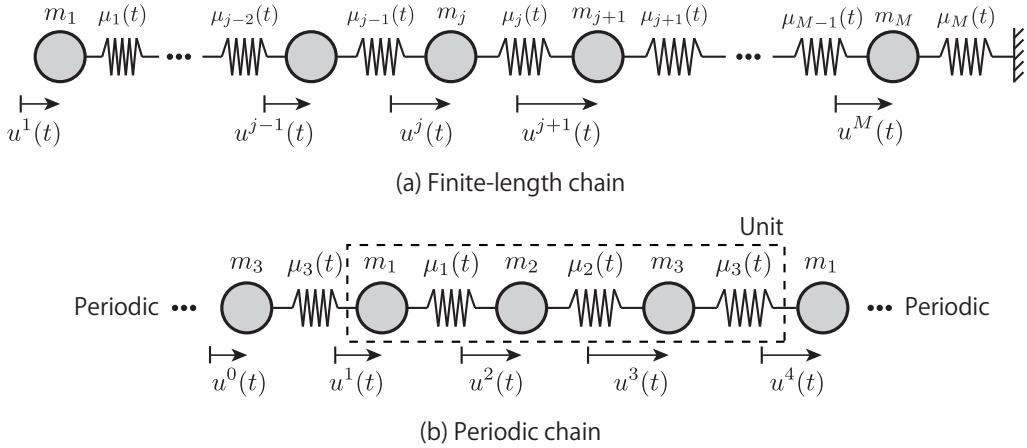


Figure 1: Chain of spring-mass pairs.

Su-Schrieffer-Heeger model [32]) in quantum physics.

As non-Hermitian mechanical systems are also subjects of intensive study, some theories have been developed and validated. Melkani and Paulose studied time-modulated discrete mechanical systems based on space-time symmetry [33]. Ghatak et al. discussed the non-Hermitian topology in an active mechanical metamaterial in analogy to the Su-Schrieffer-Heeger model [34]. A mathematical theory for time-modulated discrete systems is also established by Ammari and Kosche [18]. Nevertheless, it remains unclear how the spectrum of time-modulated dynamic mechanical systems with OBCs is associated with that of periodic lattices.

In this study, we propose a non-Bloch band theory for time-modulated discrete mechanical systems. Time-modulated mass-spring chains are formulated using the temporal Floquet theory. We present numerical evidence that the conventional Bloch band theory is not valid for the time-modulated systems. Following [29], we define a generalized Brillouin zone and establish a non-Bloch band theory. This allows us to estimate eigenvalues of long chains in the complex frequency plane even in the presence of non-Hermitian skin modes that arise from the non-reciprocity.

2. Chain of a finite number of masses and springs

2.1. Model

As shown in Figure 1 (a), we consider a chain of masses m_1, m_2, \dots, m_M connected with springs whose parameters are $\mu_1, \mu_2, \dots, \mu_M$. The parameters (stiffness) μ_1, \dots, μ_M are modulated in time while the masses are constant. The displacement u^j of each mass ($j = 1, \dots, M$) is governed by the following equations of motion:

$$m_j \partial_{tt} u^j(t) = \mu_{j-1}(t) u^{j-1}(t) - (\mu_{j-1}(t) + \mu_j(t)) u^j(t) + \mu_j u^{j+1}(t) + f_j(t) \quad (1)$$

for $j = 2, \dots, M - 1$, and

$$m_1 \partial_{tt} u^1(t) = -\mu_1(t) u^1(t) + \mu_1 u^2(t) + f_1(t), \quad (2)$$

$$m_M \partial_{tt} u^M(t) = \mu_{M-1}(t) u^{M-1}(t) - (\mu_{M-1}(t) + \mu_M) u^M(t) + f_M(t), \quad (3)$$

where f_j denotes an external force applied to the mass m_j .

Let us consider a time-harmonic excitation, i.e., for each $j = 1, \dots, M$, there exists a constant $F_j \in \mathbb{C}$ such that

$$f_j(t) = \operatorname{Re} [F_j e^{-i\omega t}] \quad (4)$$

with angular frequency $\omega \in \mathbb{R}$. In addition, we assume that the modulation of the stiffness is periodic in time with angular frequency $\Omega > 0$ and given by

$$\mu_j(t) = G_j + \gamma_j \cos(\Omega t - \phi_j) = G_j + \frac{\gamma_j}{2} e^{-i\phi_j} e^{i\Omega t} + \frac{\gamma_j}{2} e^{i\phi_j} e^{-i\Omega t} \quad (5)$$

with constants $G_j > 0$, $\gamma_j \in [0, G_j)$, and $\phi_j \in [-\pi, \pi]$. Since all the coefficients μ_j are T -periodic, i.e., $\mu_j(t+T) = \mu_j(t)$ with $T = 2\pi/\Omega$ for all $j = 1, \dots, M$ and $t \in \mathbb{R}$, we use the Floquet theory [16–18] and seek solutions u^j of the form

$$u^j(t) = \operatorname{Re} \left[e^{-i\omega t} \sum_{n=-\infty}^{\infty} U_n^j e^{-in\Omega t} \right], \quad (6)$$

$$\partial_t u^j(t) = \operatorname{Re} \left[e^{-i\omega t} \sum_{n=-\infty}^{\infty} V_n^j e^{-in\Omega t} \right] \quad (7)$$

with unknown coefficients $U_n^j, V_n^j \in \mathbb{C}$ ($n \in \mathbb{Z}$) for each $j = 1, \dots, M$. The coefficients should satisfy $(\omega + n\Omega)U_n^j = iV_n^j$ for each j and n . Note that the response u^j is not in general time-harmonic with angular frequency ω despite the harmonic excitation f_j . In view of this, the factor ω in (6) is called *quasifrequency* [17].

Inserting (4)–(6) into (1)–(3), we obtain the following linear relation for each $n \in \mathbb{Z}$:

$$\begin{aligned} & -im_j(\omega + n\Omega)V_n^j - G_{j-1}U_n^{j-1} + (G_{j-1} + G_j)U_n^j - G_jU_n^{j+1} \\ & - \bar{\eta}_{j-1}U_{n+1}^{j-1} + (\bar{\eta}_{j-1} + \bar{\eta}_j)U_{n+1}^j - \bar{\eta}_jU_{n+1}^{j+1} \\ & - \eta_{j-1}U_{n-1}^{j-1} + (\eta_{j-1} + \eta_j)U_{n-1}^j - \eta_jU_{n-1}^{j+1} = F_j\delta_{n,0}, \quad j = 2, \dots, M-1, \quad (8) \\ & -im_1(\omega + n\Omega)V_n^1 + G_1U_n^1 - G_1U_n^2 \\ & \quad + \bar{\eta}_1U_{n+1}^1 - \bar{\eta}_1U_{n+1}^2 + \eta_1U_{n-1}^1 - \eta_jU_{n-1}^2 = F_1\delta_{n,0}, \end{aligned} \quad (9)$$

$$\begin{aligned} & -im_M(\omega + n\Omega)V_n^M - G_{M-1}U_n^{M-1} + (G_{M-1} + G_M)U_n^M \\ & - \bar{\eta}_{M-1}U_{n+1}^{M-1} + (\bar{\eta}_{M-1} + \bar{\eta}_M)U_{n+1}^M \\ & - \eta_{M-1}U_{n-1}^{M-1} + (\eta_{M-1} + \eta_M)U_{n-1}^M = F_M\delta_{n,0}, \end{aligned} \quad (10)$$

where η_j is the constant defined by $\eta_j = \gamma_j e^{i\phi_j}/2$, and $\delta_{n,0}$ is the Kronecker delta, i.e.,

$$\delta_{n,0} = \begin{cases} 1 & (n = 0) \\ 0 & (n \neq 0) \end{cases}. \quad (11)$$

For numerical computation, we truncate the Fourier series in terms of n with sufficiently large integer P and approximate the linear system (8)–(10) into

$$\left(\begin{bmatrix} \mathbf{K} & -i\Omega\mathbf{MB} \\ i\Omega\mathbf{MB} & \mathbf{M} \end{bmatrix} - \omega \begin{bmatrix} \mathbf{O} & i\mathbf{M} \\ -i\mathbf{M} & \mathbf{O} \end{bmatrix} \right) \begin{pmatrix} \mathbf{U} \\ \mathbf{V} \end{pmatrix} = \begin{pmatrix} \mathbf{F} \\ \mathbf{0} \end{pmatrix}, \quad (12)$$

where the matrices are defined by

$$\mathbf{K} = \begin{bmatrix} K_1 & -K_1 & & & & \\ -K_1 & K_1 + K_2 & -K_2 & & & \\ & -K_2 & K_2 + K_3 & -K_3 & & \\ & & & \ddots & & \\ & & & & -K_{M-1} & K_{M-1} + K_M \end{bmatrix}, \quad (13)$$

$$\mathbf{M} = \text{diag}(m_1I, m_2I, \dots, m_MI), \quad (14)$$

$$\mathbf{B} = \text{diag}(B, B, \dots, B) \quad (15)$$

with submatrices

$$K_j = \begin{bmatrix} G_j & \bar{\eta}_j & & & \\ \eta_j & G_j & \bar{\eta}_j & & \\ & \eta_j & G_j & \bar{\eta}_j & \\ & & & \ddots & \\ & & & & \eta_j & G_j \end{bmatrix}, \quad B = \text{diag}(-P, -P + 1, \dots, P - 1, P). \quad (16)$$

Analogously, the vectors are associated with the constants and Fourier coefficients as follows:

$$U = (U_{-P}^1, \dots, U_0^1, \dots, U_P^1, \dots, U_{-P}^M, \dots, U_0^M, \dots, U_P^M)^T, \quad (17)$$

$$V = (V_{-P}^1, \dots, V_0^1, \dots, V_P^1, \dots, V_{-P}^M, \dots, V_0^M, \dots, V_P^M)^T, \quad (18)$$

$$F = (0, \dots, F_1, \dots, 0, \dots, 0, \dots, F_N, \dots, 0)^T. \quad (19)$$

Note that the matrix product

$$\mathcal{H} := \begin{bmatrix} O & iM \\ -iM & O \end{bmatrix}^{-1} \begin{bmatrix} K & -i\Omega MB \\ i\Omega MB & M \end{bmatrix} \quad (20)$$

is not necessarily Hermitian despite that each matrix is Hermitian. Thus, we cannot always expect that eigenvalues ω of \mathcal{H} are all real. However, due to the Hermiticity of the two matrices, it can be proved that the eigenvalues ω are real or come in complex-conjugate pairs $(\omega, \bar{\omega})$ [35].

2.2. Numerical example

We first check that the Floquet theory is valid for the time-modulated system. As shown in Figure 2 (a), we consider the mass-spring pairs with $M = 2$. The masses are set to $m_1 = m_2 = m$ with given $m > 0$, and the stiffness is given by $\mu_1(t) = G$ and $\mu_2(t) = G + G\delta \cos(\Omega t - \pi/4)$ for some $G > 0$ and $\delta \in [0, 1)$ (i.e., $\gamma_1 = 0$, $\gamma_2 = G\delta$, and $\phi_2 = \pi/4$). The modulation angular frequency is $\Omega = 0.9\omega_0$, where $\omega_0 = \sqrt{G/m}$ is the resonant frequency of the single mass-spring pair. For numerical computation, the Fourier series in terms of $n \in \mathbb{Z}$ are truncated into $n = -4, \dots, 4$, i.e., $P = 4$.

Figure 2 (b) and (c) show the trajectories of eigenvalues ω of \mathcal{H} as the modulation amplitude δ varies from 0 to 0.99. As the spectrum is Ω -periodic in the complex ω -plane [17], we plot eigenvalues only within the range of $0 \leq$

$\text{Re}[\omega] \leq \Omega$. The results indicate that all the eigenvalues are purely real when the modulation amplitude δ is less than 0.843. Above this threshold, the eigenvalues come in a conjugate pair $(\omega, \bar{\omega})$ with nonzero imaginary part. The eigenvalues with negative and positive imaginary part are associated with modes decaying and growing in time, respectively (recall that the convention $e^{-i\omega t}$ is used). This means that the system undergoes a phase transition from stable to unstable states. This is a typical phenomenon in PT symmetric systems and called real-to-complex eigenvalue transition, pseudo-Hermiticity breaking, or PT phase transition [33, 36].

We compare the results of the eigenvalue analysis with numerical solutions of (1)–(3). As (1)–(3) are just a linear system of ordinary differential equations, we use the backward Euler method to stably compute its numerical solution. The temporal discretization is given by $t = 0, \Delta t, 2\Delta t, \dots$ with $\Delta t = T/5000$. Figure 2 (d) shows numerical solutions $u^1(t)$ and $u^2(t)$ when the initial conditions are given by $u^1(0) = u_0$ and $u^2(0) = \partial_t u^1(0) = \partial_t u^2(0) = 0$ for some $u_0 > 0$. For $\delta = 0.835$, it is clear that the oscillation is stable in time. In the case of $\delta = 0.850$, the displacements grow exponentially in time. This is consistent with the discussion from the Floquet theory. Moreover, their growth rate $1/\tau$ is almost the same with the imaginary part of the eigenvalue ω obtained from the Floquet theory (see Figure 2 (c)). From these results, we conclude that the Floquet theory is valid for the time-modulated mechanical system.

We are interested in the spectrum of time-modulated chains with large M . As shown in Figure 3 (a) and (b), we consider the chain of length $M = 300$ with the following parameters:

$$\Omega = 1.8\omega_0, \quad m_1 = \dots = m_{300} = m, \quad \gamma_1 = \dots = \gamma_{300} = 0.2G, \quad (21)$$

$$G_{3j-2} = G, \quad G_{3j-1} = 0.75G, \quad G_{3j} = G \quad (j = 1, \dots, 100), \quad (22)$$

$$\phi_{3j-2} = 0, \quad \phi_{3j-1} = \pi, \quad \phi_{3j} = \pi/2 \quad (j = 1, \dots, 100). \quad (23)$$

Figure 3 (c) shows the distribution of the eigenvalues ω of \mathcal{H} . In analogy with the previous results with $M = 2$, the spectrum is symmetric with respect to the real axis. In addition, the spectrum accumulates along some curves in the complex ω -plane.

In Figure 3 (d), we plot eigenmodes corresponding to some eigenvalues in the spectrum. The eigenmodes A, B, and C (and their conjugate pairs) exponentially grow as the site index j increases or decreases. This means that some modes are localized at either left or right edge of the chain. The other

modes D and E (purely real eigenvalues) are almost uniformly distributed in space. This localization deserves a careful investigation as the usual mass-spring chains do not exhibit such spatial behaviors.

3. Non-Bloch band theory

In the previous section, we observed that the long chain with repeating units exhibit some special spectral structures and its eigenmodes can be localized at the edges. To analyze these unique properties, we approximate the long chain as a purely periodic system. The interesting point is that the standard Bloch band theory breaks down for our time-modulated system due to the non-Hermiticity of \mathcal{H} . In this section, we introduce the non-Bloch band theory [28, 29] with a generalized Brillouin zone [25, 30] to study the spectrum of \mathcal{H} for long chains with OBCs.

3.1. Bloch band theory with Brillouin zone

As shown in Figure 1 (b), we consider a periodic chain of masses and springs. The unit of the chain comprises three masses (m_1, m_2, m_3) connected with springs characterized by (μ_1, μ_2, μ_3) . As in the previous section, the masses are constant in time, and the stiffness μ_j is modulated as (5) using constants G_j , γ_j , and ϕ_j for $j = 1, 2, 3$. Since we are interested in the spectrum, the external force is set to $f_j = 0$. For each $j \in \mathbb{Z}$, the displacement u^j satisfies the equation of motion (1). The periodicity with respect to time t allows us to use the Floquet condition (6). In addition, since the system is now also periodic in space, the Bloch theory states that a solution is quasi-periodic in space, i.e., there exists a scalar k (Bloch wavenumber) such that

$$U_n^{j+3} = U_n^j e^{ik} \quad (24)$$

for all $j \in \mathbb{Z}$. Then, we arrive at the following linear system

$$\left(\begin{bmatrix} \mathbf{K}_k & -i\Omega \mathbf{MB} \\ i\Omega \mathbf{MB} & \mathbf{M} \end{bmatrix} - \omega \begin{bmatrix} \mathbf{O} & i\mathbf{M} \\ -i\mathbf{M} & \mathbf{O} \end{bmatrix} \right) \begin{pmatrix} \mathbf{U} \\ \mathbf{V} \end{pmatrix} = \begin{pmatrix} \mathbf{0} \\ \mathbf{0} \end{pmatrix}, \quad (25)$$

where the matrix \mathbf{K}_k is defined by

$$\mathbf{K}_k = \begin{bmatrix} K_3 + K_1 & -K_1 & -K_3 e^{-ik} \\ -K_1 & K_1 + K_2 & -K_2 \\ -K_3 e^{ik} & -K_2 & K_2 + K_3 \end{bmatrix}, \quad (26)$$

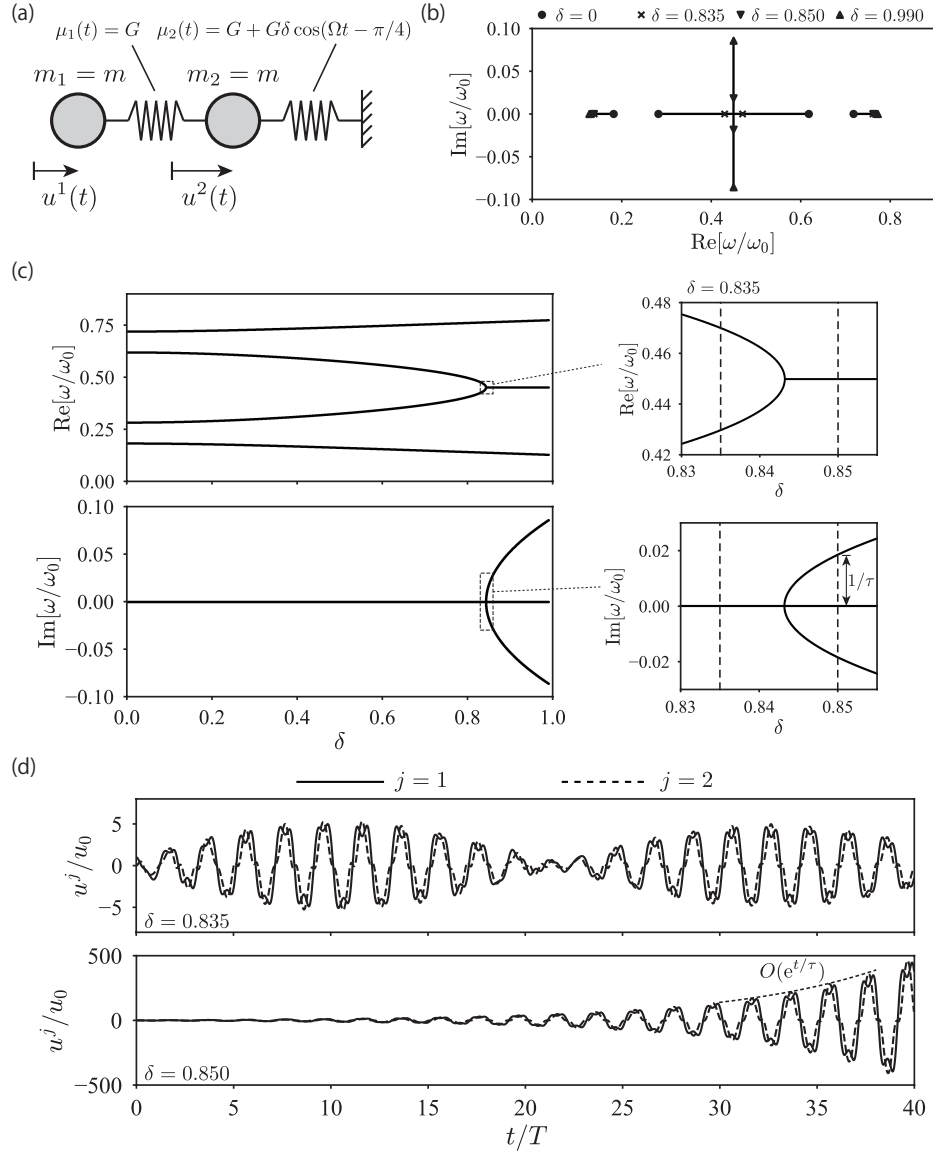


Figure 2: Verification of the Floquet theory for a time-modulated system. (a) Two mass-spring pairs. (b), (c) Trajectory of eigenvalues ω as the modulation amplitude δ varies from 0 to 0.99. (d) displacements u^1 and u^2 as a function of time t when the initial conditions $u^1(0) = u_0$ and $u^2(0) = \partial_t u^1(0) = \partial_t u^2(0) = 0$ are given.

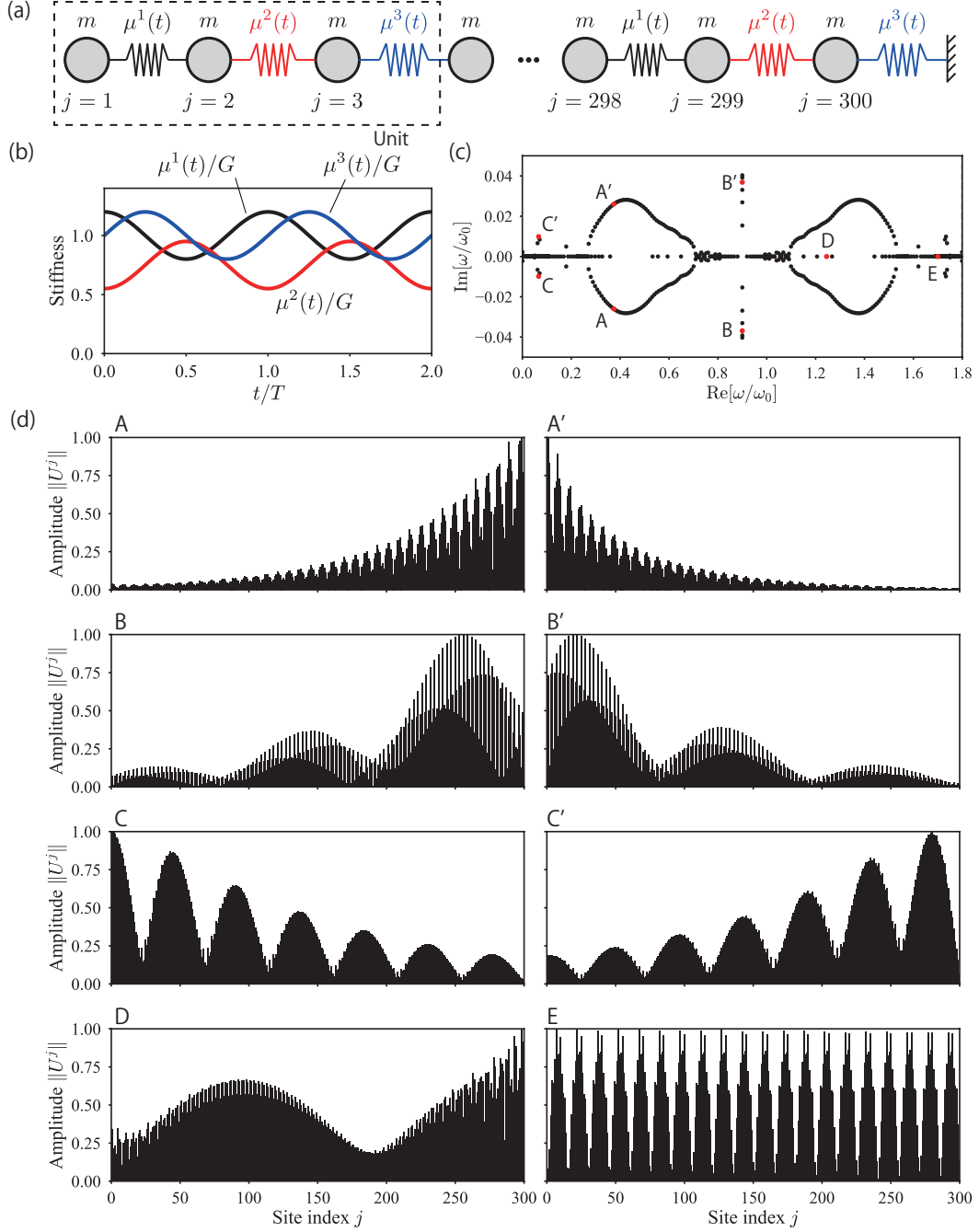


Figure 3: Spectrum of \mathcal{H} for a long-chain of mass-spring pairs. (a) A long chain consists of spatially periodic units. Its unit comprises three mass-spring pairs. (b) Time modulation of μ^1 , μ^2 , and μ^3 . (c) Distribution of eigenvalues ω for the system (a). Some representatives are denoted by the symbols A, B, C, D, and E with their conjugate pairs. (d) Eigenmodes corresponding to the representatives.

and the other matrices and vectors are as in the previous section with $M = 3$.

For fixed k , the system (25) can be rewritten as $\mathcal{H}_k\varphi = \omega\varphi$ with vector φ and square matrix (Bloch Hamiltonian)

$$\mathcal{H}_k := \begin{bmatrix} O & i\mathbf{M} \\ -i\mathbf{M} & O \end{bmatrix}^{-1} \begin{bmatrix} \mathbf{K}_k & -i\Omega\mathbf{MB} \\ i\Omega\mathbf{MB} & \mathbf{M} \end{bmatrix}, \quad (27)$$

which depends on k . Let $\sigma(k) = \{\omega \in \mathbb{C} : \det(\omega I - \mathcal{H}_k) = 0\}$ be the spectrum of \mathcal{H}_k . The union $\sigma_{\text{BZ}} := \cup_{k \in \mathbb{R}} \sigma(k)$ is called a Bloch band. For the computation of σ_{BZ} , it suffices to consider $k \in [-\pi, \pi]$ as the 2π shift does not affect the Bloch condition (24), i.e., $\mathcal{H}_{k+2\pi} = \mathcal{H}_k$ and $\sigma_{\text{BZ}} = \cup_{k \in [-\pi, \pi]} \sigma(k)$. The range $[-\pi, \pi]$ is called the (first) Brillouin zone (BZ).

For Hermitian systems (e.g. $\gamma_j = 0$), it is well known that the Bloch band σ_{BZ} is an approximation to the spectrum $\sigma_{\text{OBC}} := \{\omega \in \mathbb{C} : \det(\omega I - \mathcal{H}) = 0\}$ of the long chain (sufficiently large M) with OBCs, discussed in the previous section. Namely, the OBCs can be regarded as a small perturbation to the purely periodic system without edges.

However, this well-known fact does not always hold true for non-Hermitian systems [27]. The Bloch condition (24) with real k implicitly enforces solutions not to grow or decay in space, which is not a reasonable assumption from the results in Figure 3 (d).

To see this, we present a numerical example of the Bloch band σ_{BZ} in Figure 4. As shown in Figure 4 (a) and (b), we use the same modulation frequency Ω and material parameters m_j , G_j , γ_j , and ϕ_j in (21)–(23). Figure 4 (c) and (d) show the Bloch band diagram on the Brillouin zone $-\pi \leq k \leq \pi$. As the periodic system is also non-Hermitian, the eigenvalues of \mathcal{H}_k are complex-valued in general. Notably, the bands are asymmetric with respect to the inversion $k \rightarrow -k$, which implies that the system is non-reciprocal. Figure 4 (e) shows the comparison between the bands σ_{BZ} and spectrum of the long chain σ_{OBC} in Figure 3 (c). From the result, we observe the obvious discrepancy between the two spectra. This implies that the Bloch band theory with the standard BZ does not work for our time-modulated system.

3.2. Non-Bloch band theory with generalized Brillouin zone

To deal with eigenmodes growing and decaying in space, we need to allow the Bloch wavenumber k to be complex. Following the common notation, we

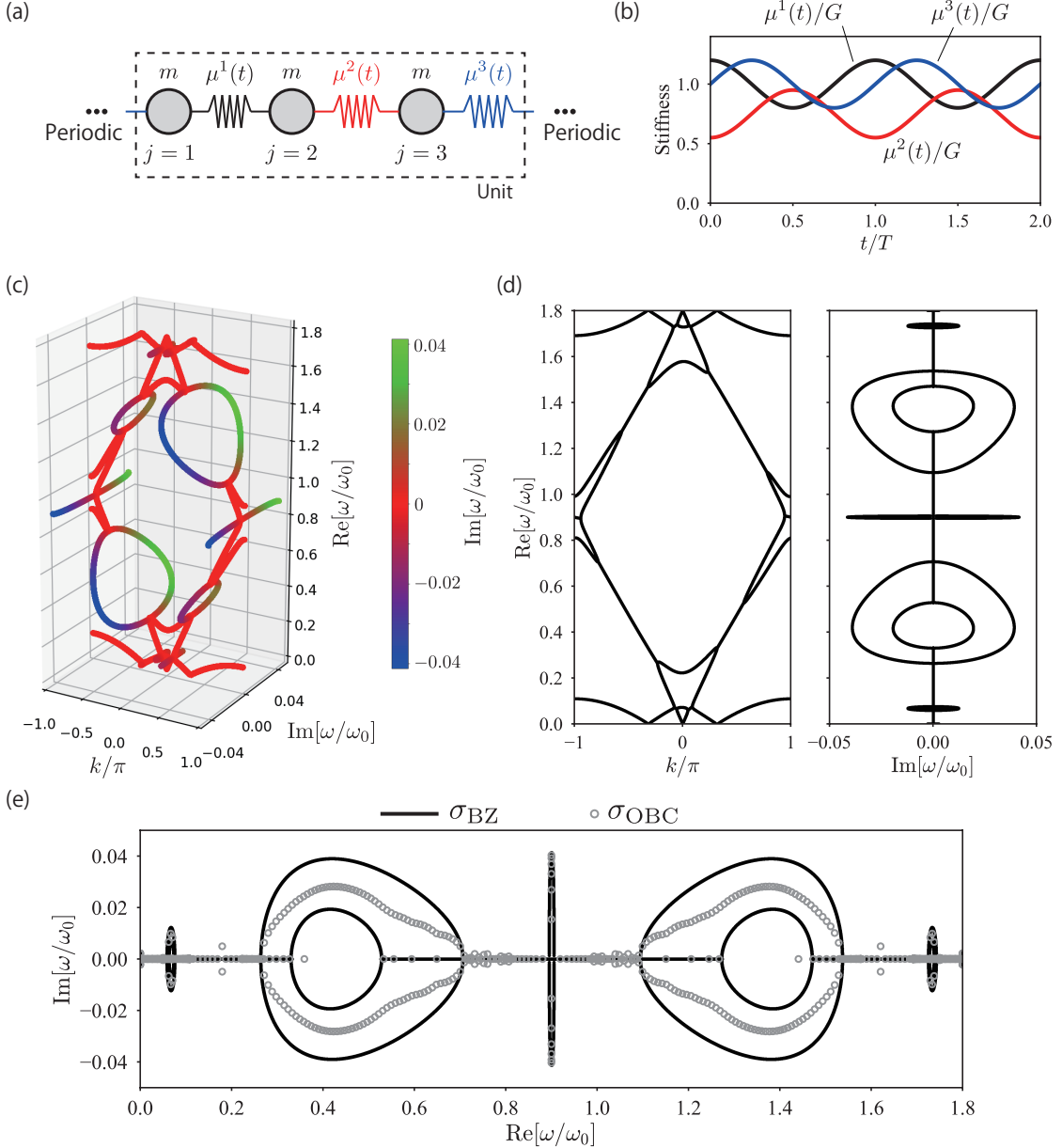


Figure 4: Bloch band σ_{BZ} and OBC spectrum σ_{OBC} . (a), (b) Periodic chain of mass-spring pairs. The unit of the chain is the same as in Figure 3 (a), (b). (c), (d) $\sigma(k)$ as a function of $k \in [-\pi, \pi]$ (Bloch band diagram). (e) Comparison between σ_{BZ} and σ_{OBC} in Figure 3.

define $\beta = e^{ik}$. Then, the linear system (25) is rewritten as

$$\left(\begin{bmatrix} \mathbf{P}_0 - \beta \mathbf{P}_1 - \beta^{-1} \mathbf{P}_{-1} & -i\Omega \mathbf{MB} \\ i\Omega \mathbf{MB} & \mathbf{M} \end{bmatrix} - \omega \begin{bmatrix} \mathbf{O} & i\mathbf{M} \\ -i\mathbf{M} & \mathbf{O} \end{bmatrix} \right) \begin{pmatrix} \mathbf{U} \\ \mathbf{V} \end{pmatrix} = \begin{pmatrix} \mathbf{0} \\ \mathbf{0} \end{pmatrix}, \quad (28)$$

where the matrices \mathbf{P}_0 , \mathbf{P}_1 , and \mathbf{P}_{-1} are defined by

$$\mathbf{P}_0 = \begin{bmatrix} K_3 + K_1 & -K_1 & \mathbf{O} \\ -K_1 & K_1 + K_2 & -K_2 \\ \mathbf{O} & -K_2 & K_2 + K_3 \end{bmatrix}, \quad (29)$$

$$\mathbf{P}_1 = \begin{bmatrix} \mathbf{O} & \mathbf{O} & \mathbf{O} \\ \mathbf{O} & \mathbf{O} & \mathbf{O} \\ K_3 & \mathbf{O} & \mathbf{O} \end{bmatrix}, \quad \mathbf{P}_{-1} = \begin{bmatrix} \mathbf{O} & \mathbf{O} & K_3 \\ \mathbf{O} & \mathbf{O} & \mathbf{O} \\ \mathbf{O} & \mathbf{O} & \mathbf{O} \end{bmatrix}. \quad (30)$$

The system (28) yields a (generalized) linear eigenvalue problem in terms of ω for fixed $\beta \in \mathbb{C}$. When $\omega \in \mathbb{C}$ is given, this is a quadratic eigenvalue problem in terms of β , which can be recast into a linear eigenvalue problem [35].

For each $\omega \in \mathbb{C}$, let $\beta_1(\omega), \beta_2(\omega), \dots, \beta_{2N}(\omega)$ be eigenvalues of (28), where N is the size of the partitioned matrices in (28). The eigenvalues are sorted such that $|\beta_1(\omega)| \leq |\beta_2(\omega)| \leq \dots \leq |\beta_{2N}(\omega)|$. A generalized Brillouin zone (GBZ) [25, 30] is defined by

$$C_{\text{GBZ}} = \{\beta_N(\omega) : \omega \in \sigma_{\text{GBZ}}\} \cup \{\beta_{N+1}(\omega) : \omega \in \sigma_{\text{GBZ}}\}, \quad (31)$$

with

$$\sigma_{\text{GBZ}} = \{\omega \in \mathbb{C} : |\beta_N(\omega)| = |\beta_{N+1}(\omega)|\}. \quad (32)$$

The non-Bloch band theory claims that the set σ_{GBZ} is an approximation to the spectrum of \mathcal{H} with repeating units and large M (e.g. Figure 3 (a)).

To see this, for a fixed $\omega \in \mathbb{C}$ and $F = 0$, we consider a solution of (12) of the form

$$\begin{pmatrix} \mathbf{U}^{3j-2} \\ \mathbf{V}^{3j-2} \end{pmatrix} = (\beta^{(1)})^{j-1} \varphi^{(1)} + (\beta^{(2)})^{j-1} \varphi^{(2)} \quad (33)$$

for each j , where $\beta^{(1)}$ and $\beta^{(2)}$ are eigenvalues of (28) with $|\beta^{(1)}| \leq |\beta^{(2)}|$. The vectors $\varphi^{(1)}$ and $\varphi^{(2)}$ should be determined from OBCs. For simplicity, let us consider the clamped boundary condition at the left and right edges,

i.e., $(U^1, V^1) = (U^{3M-2}, V^{3M-2}) = 0$. Then, we arrive at the characteristic equation

$$\det \begin{bmatrix} I & I \\ (\beta^{(1)})^{M-1} I & (\beta^{(2)})^{M-1} I \end{bmatrix} = 0 \quad (34)$$

or equivalently $(\beta^{(1)})^{M-1} - (\beta^{(2)})^{M-1} = 0$. If $|\beta^{(1)}| < |\beta^{(2)}|$, then this implies that both $\beta^{(1)}$ and $\beta^{(2)}$ tend to 0 as $M \rightarrow \infty$. This contradicts that $\beta^{(1)}$ and $\beta^{(2)}$ are eigenvalues of (28). Therefore, we need to impose the condition $|\beta^{(1)}| = |\beta^{(2)}|$, i.e., $|\beta_N| = |\beta_{N+1}|$.

We numerically show that this non-Bloch band theory predicts the spectrum of the finite-length time-modulated system. We use the same parameters and compute $\beta^{(1)} = \beta_N$ and $\beta^{(2)} = \beta_{N+1}$ for varying $\omega \in \mathbb{C}$. The results are plotted in Figure 5 (a) and indicate that the contour $|\beta^{(1)}(\omega)| = |\beta^{(2)}(\omega)|$ (i.e. σ_{GBZ}) forms a continuous curve with several branches in the complex ω -plane, which resembles the finite-chain spectrum σ_{OBC} in Figure 3 (c). In fact, Figure 5 (b) shows that almost all the eigenvalues in σ_{OBC} lie on the contour σ_{GBZ} . Figure 5 (d) shows C_{GBZ} calculated from the spectrum σ_{GBZ} . In contrast to the standard BZ (unit circle $|\beta| = 1$), the GBZ deviates from the circle, which suggests the existence of non-Hermitian skin effects [25]. An eigenmode corresponding to an eigenvalue $\omega \in \sigma_{\text{GBZ}}$ is called a non-Hermitian skin mode if $|\beta_N(\omega)| = |\beta_{N+1}(\omega)| \neq 1$. For example, the eigenvalue A in Figure 5 (b) lies on the spectrum σ_{GBZ} with $|\beta| > 1$. This implies that the corresponding eigenmode grows exponentially as the site index j increases. In fact, the finite-length chain exhibits a growing eigenmode at A as we have seen in Figure 3 (d). The same discussion is valid for other eigenvalues B, C, D, E, and their conjugate pairs, i.e., the non-Bloch band theory with the GBZ tells whether a given eigenvalue is associated with a mode localized at the edges (non-Hermitian skin mode) or extending in the bulk (usual Bloch mode).

Time modulation gives rise to non-Hermitian degeneracy of eigenvalues. In the zoom-in views in Figure 5 (b) and (c), we mark some representative points F, G, H, I, and J. When the eigenvalues $\omega \in \sigma_{\text{GBZ}}$ are seen as a function of β , we can observe that two eigenvalues ω degenerate at around the point I. Numerical experiments show that the matrix \mathcal{H}_k has two degenerate eigenvalues $\omega/\omega_0 = 0.32998$ at $k = 0.99805$ ($\beta = 0.54194 + 0.84042i$). We calculated the ℓ^2 inner product between the corresponding eigenvectors φ_1 and φ_2 and obtained $|(\varphi_1/\|\varphi_1\|_{\ell^2}, \varphi_2/\|\varphi_2\|_{\ell^2})_{\ell^2}| = 0.0974$, which implies that

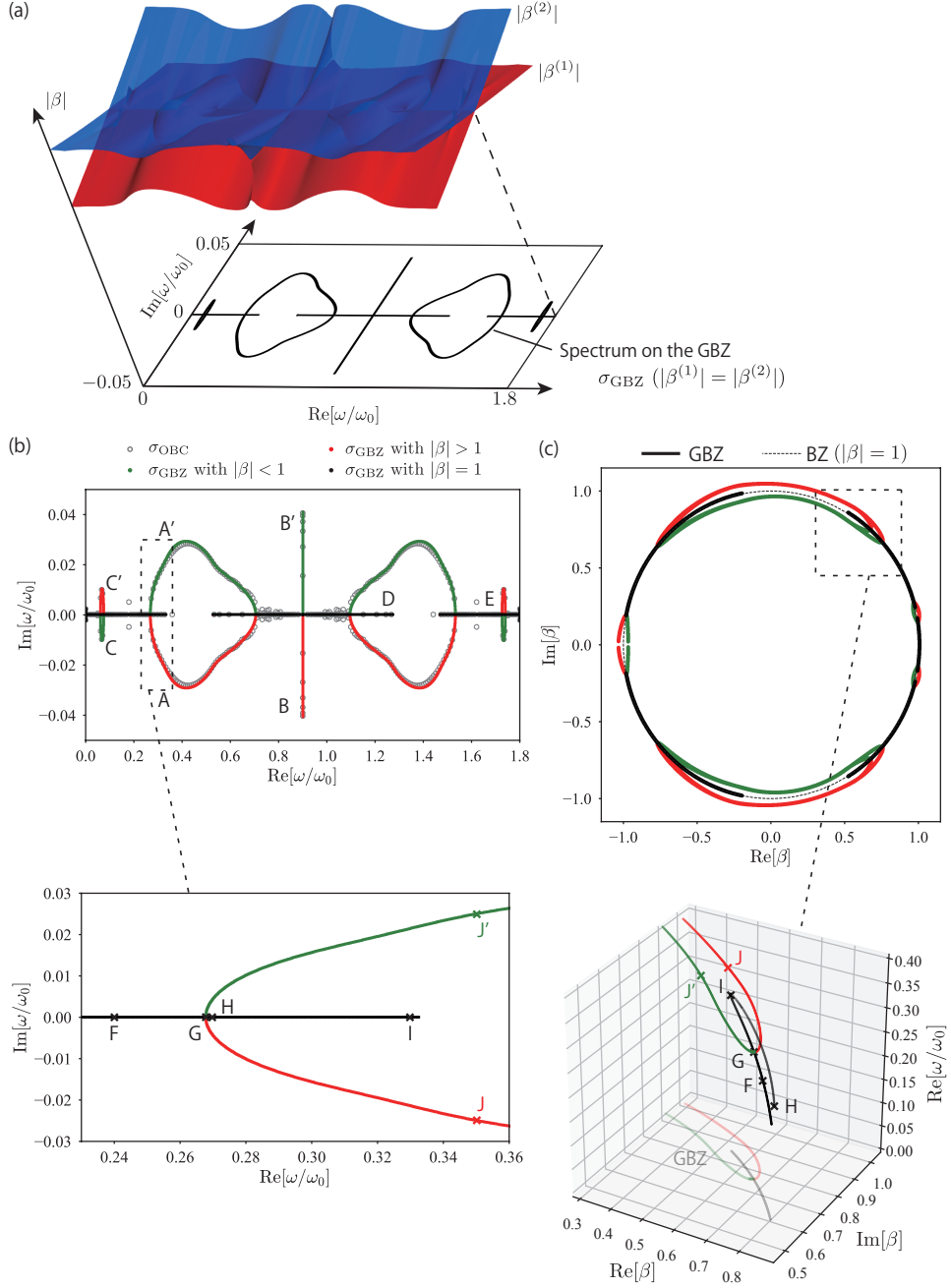


Figure 5: Non-Bloch band theory for the periodic chain shown in Figure 4 (a). (a) Eigenvalues $\beta(\omega)$ of (28) as a function of $\omega \in \mathbb{C}$. The contour $|\beta^{(1)}(\omega)| = |\beta^{(2)}(\omega)|$ is shown in the complex ω -plane. (b) Comparison between the GBZ spectrum σ_{GBZ} and σ_{OBC} shown in Figure 3. (c) C_{GBZ} in the complex β -plane. The red, green, and black lines represent $|\beta| > 1$, $|\beta| < 1$, and $|\beta| = 1$, respectively.

the eigenvectors are non-orthogonal in the ℓ^2 sense. This cannot be observed in non-modulated systems as the matrix (operator) \mathcal{H}_k is Hermitian (self-adjoint in ℓ^2).

3.3. Transient wave motion

We finally discuss the transient wave motion in the time-modulated system. As shown in Figure 3 (a), we consider the finite-length chain with $M = 300$ and the same parameters in Section 2.2.

Here, we numerically solve the system of ordinary differential equations (1)–(3) using the backward Euler method with time increment $T/1000$, as we have done in Section 2.2. The initial condition is set to $u^j = 0$ and $\partial_t u^j = 0$ for all $j = 1, \dots, M$. A time-harmonic external force is applied at the center of the chain with $M = 300$, i.e.,

$$f_j(t) = \begin{cases} A \cos \omega_f t & (j = 151) \\ 0 & (\text{otherwise}) \end{cases} \quad (35)$$

with the angular frequency $\omega_f = 0.31\omega_0$ and constant amplitude $A > 0$.

Figure 6 shows the displacements u^j at some time steps. The mechanical waves excited by the external force propagate both in the left and right directions. While the right-propagating wave almost preserves its amplitudes, the left-propagating wave rapidly grows in time before reaching the edge. This asymmetric (non-reciprocal) propagation can be explained using the non-Bloch band theory. Table 1 lists some eigenvalues β of (28) and corresponding wavenumber k for $\omega = \omega_f$. The table indicates that the system has only two eigenvalues β with $|\beta| = 1$ (or equivalently $\text{Im}[k] = 0$). As both the two eigenvalues β_N and β_{N+1} has positive imaginary part (positive real part in k_N and k_{N+1}), the array supports no propagating waves with constant amplitude (Bloch modes) in the left direction. The other eigenvalues β_{N-1} and β_{N+2} stand for left-propagating waves with growing and decaying in space (non-Hermitian skin modes), respectively. This is consistent with the transient wave motion in Figure 6.

4. Concluding remarks

In this study, we proposed a non-Bloch band theory for estimating eigenvalue distribution of time-modulated mechanical systems. The temporal Floquet theory revealed an analogy with non-Hermitian physics in quantum mechanics and suggested the breakdown of the conventional Bloch band theory.

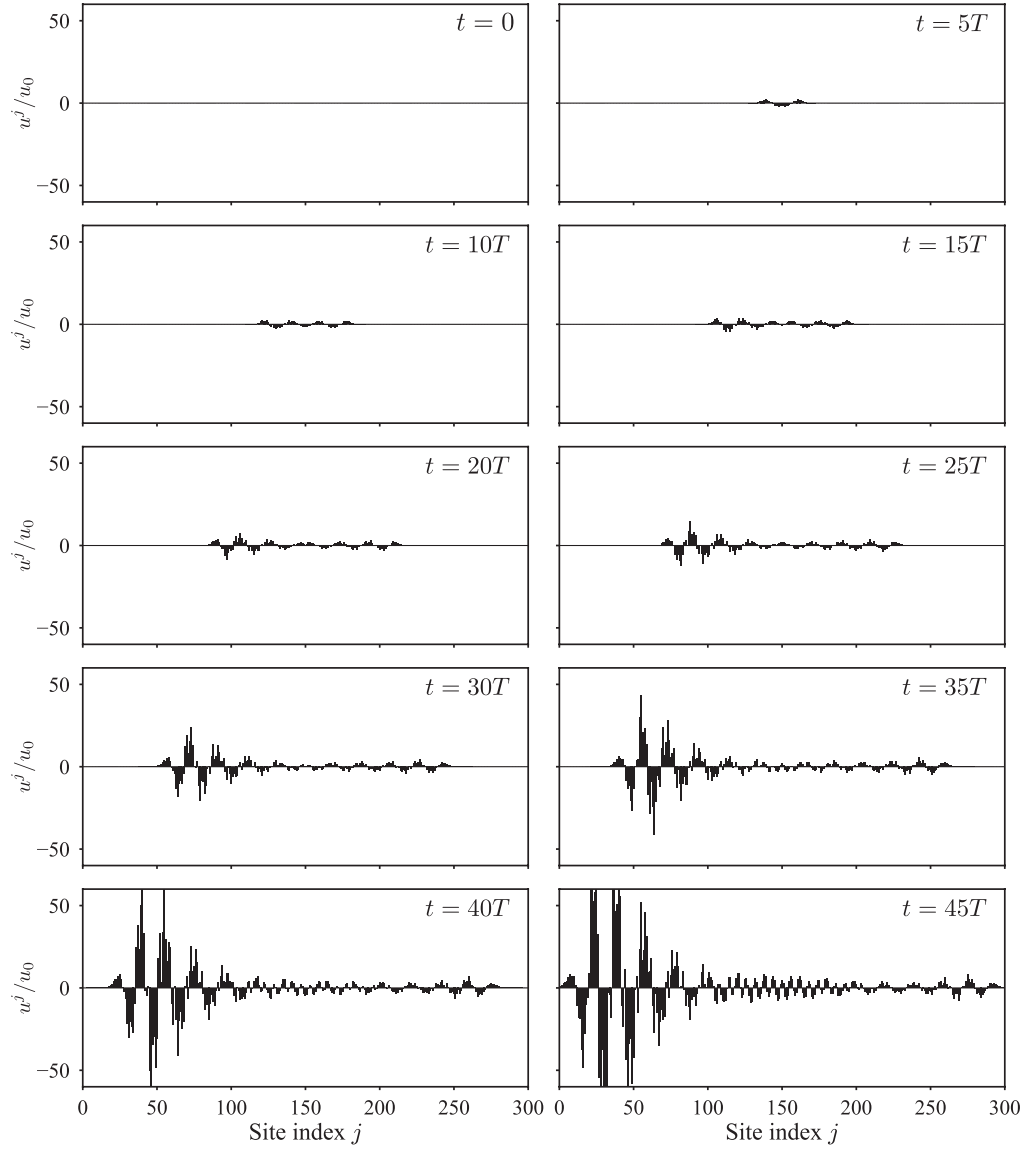


Figure 6: Transient wave motion in the finite-length chain shown in Figure 3 (a) at some time steps. The displacements u^j are normalized by $u_0 := A/G$.

Table 1: Eigenvalues β of (28) at $\omega = \omega_f$.

r	β_r	$k_r = -i \log \beta_r$
$N - 1$	$5.564 \times 10^{-1} - 6.880 \times 10^{-1}i$	$-8.908 \times 10^{-1} + 1.223 \times 10^{-1}i$
N	$5.748 \times 10^{-1} + 8.183 \times 10^{-1}i$	$9.584 \times 10^{-1} + 2.656 \times 10^{-14}i$
$N + 1$	$6.850 \times 10^{-1} + 7.286 \times 10^{-1}i$	$8.163 \times 10^{-1} - 2.504 \times 10^{-14}i$
$N + 2$	$7.106 \times 10^{-1} - 8.787 \times 10^{-1}i$	$-8.908 \times 10^{-1} - 1.223 \times 10^{-1}i$

We presented some numerical examples and observed significant discrepancy between the spectra of finite and periodic systems due to the presence of non-Hermitian skin effects. To deal with such localized modes, we proposed a non-Bloch band theory based on a GBZ. Numerical experiments showed that the results from the proposed theory are consistent with the spectrum for a finite-length chain and transient wave motion calculated using the backward Euler scheme.

Acknowledgements

This work was supported by JSPS KAKENHI Grant Numbers 24K17191, 23H03413, 23H03798. KM acknowledges support from Mizuho Foundation for the Promotion of Sciences.

References

- [1] D. L. Sounas, A. Alù, Non-reciprocal photonics based on time modulation, *Nature Photonics* 11 (12) (2017) 774–783.
- [2] R. Fleury, D. Sounas, M. R. Haberman, A. Alù, Nonreciprocal acoustics, *Acoustics Today* 11 (3) (2015) 14–21.
- [3] H. Nassar, B. Yousefzadeh, R. Fleury, M. Ruzzene, A. Alù, C. Daraio, A. N. Norris, G. Huang, M. R. Haberman, Nonreciprocity in acoustic and elastic materials, *Nature Reviews Materials* 5 (9) (2020) 667–685.
- [4] M. B. Zanjani, A. R. Davoyan, A. M. Mahmoud, N. Engheta, J. R. Lukes, One-way phonon isolation in acoustic waveguides, *Applied Physics Letters* 104 (8) (2014) 081905. doi:10.1063/1.4866590.

- [5] Z. Chen, Y. Peng, H. Li, J. Liu, Y. Ding, B. Liang, X.-F. Zhu, Y. Lu, J. Cheng, A. Alù, Efficient nonreciprocal mode transitions in spatiotemporally modulated acoustic metamaterials, *Science Advances* 7 (45) (2021) eabj1198. doi:10.1126/sciadv.abj1198.
- [6] B. Liang, B. Yuan, J.-c. Cheng, Acoustic diode: Rectification of acoustic energy flux in one-dimensional systems, *Phys. Rev. Lett.* 103 (2009) 104301. doi:10.1103/PhysRevLett.103.104301.
- [7] Y. Chen, X. Li, H. Nassar, A. N. Norris, C. Daraio, G. Huang, Nonreciprocal wave propagation in a continuum-based metamaterial with space-time modulated resonators, *Phys. Rev. Appl.* 11 (2019) 064052. doi:10.1103/PhysRevApplied.11.064052.
- [8] K. Yi, S. Karkar, M. Collet, One-way energy insulation using time-space modulated structures, *Journal of Sound and Vibration* 429 (2018) 162–175. doi:10.1016/j.jsv.2018.05.017.
- [9] P. Wang, L. Lu, K. Bertoldi, Topological phononic crystals with one-way elastic edge waves, *Phys. Rev. Lett.* 115 (2015) 104302. doi:10.1103/PhysRevLett.115.104302.
- [10] H. Nassar, H. Chen, A. N. Norris, M. R. Haberman, G. L. Huang, Non-reciprocal wave propagation in modulated elastic metamaterials, *Proceedings of the Royal Society A: Mathematical, Physical and Engineering Sciences* 473 (2202) (2017) 20170188. doi:10.1098/rspa.2017.0188.
- [11] N. Swinteck, S. Matsuo, K. Runge, J. O. Vasseur, P. Lucas, P. A. Deymier, Bulk elastic waves with unidirectional backscattering-immune topological states in a time-dependent superlattice, *Journal of Applied Physics* 118 (6) (2015) 063103. doi:10.1063/1.4928619.
- [12] Y. Wang, B. Yousefzadeh, H. Chen, H. Nassar, G. Huang, C. Daraio, Observation of nonreciprocal wave propagation in a dynamic phononic lattice, *Phys. Rev. Lett.* 121 (2018) 194301. doi:10.1103/PhysRevLett.121.194301.
- [13] J. Vila, R. K. Pal, M. Ruzzene, G. Trainiti, A Bloch-based procedure for dispersion analysis of lattices with periodic time-varying properties,

Journal of Sound and Vibration 406 (2017) 363–377. doi:10.1016/j.jsv.2017.06.011.

- [14] A. Melkani, J. Paulose, Space-time symmetry and parametric resonance in dynamic mechanical systems, arXiv preprint arXiv:2310.08734 (2023).
- [15] X. Pu, A. Marzani, A. Palermo, A multiple scattering formulation for elastic wave propagation in space-time modulated metamaterials, Journal of Sound and Vibration 573 (2024) 118199. doi:10.1016/j.jsv.2023.118199.
- [16] H. Ammari, J. Cao, E. O. Hiltunen, Nonreciprocal wave propagation in space-time modulated media, Multiscale Modeling & Simulation 20 (4) (2022) 1228–1250. doi:10.1137/21M1449427.
- [17] H. Ammari, J. Cao, E. O. Hiltunen, L. Rueff, Transmission properties of time-dependent one-dimensional metamaterials, Journal of Mathematical Physics 64 (12) (2023) 121502. doi:10.1063/5.0143778.
- [18] H. Ammari, T. Kosche, Topological phenomena in honeycomb floquet metamaterials, Mathematische Annalen 388 (3) (2024) 2755–2785.
- [19] C. E. Rüter, K. G. Makris, R. El-Ganainy, D. N. Christodoulides, M. Segev, D. Kip, Observation of parity-time symmetry in optics, Nature physics 6 (3) (2010) 192–195.
- [20] K. Matsushima, Y. Noguchi, T. Yamada, Unidirectional invisibility in a pt-symmetric structure designed by topology optimization, Optics Letters 47 (13) (2022) 3315–3318. doi:10.1364/OL.460488.
- [21] M.-A. Miri, A. Alù, Exceptional points in optics and photonics, Science 363 (6422) (2019) eaar7709. doi:10.1126/science.aar7709.
- [22] K. Matsushima, Y. Noguchi, T. Yamada, Exceptional points in cylindrical elastic media with radiation loss, Phys. Rev. B 107 (2023) 144104. doi:10.1103/PhysRevB.107.144104.
- [23] N. Even, B. Nennig, G. Lefebvre, E. Perrey-Debain, Experimental observation of exceptional points in coupled pendulums, Journal of Sound and Vibration 575 (2024) 118239. doi:10.1016/j.jsv.2024.118239.

- [24] Y. Ashida, Z. Gong, M. Ueda, Non-Hermitian physics, *Advances in Physics* 69 (3) (2020) 249–435. doi:10.1080/00018732.2021.1876991.
- [25] S. Yao, Z. Wang, Edge states and topological invariants of non-hermitian systems, *Phys. Rev. Lett.* 121 (2018) 086803. doi:10.1103/PhysRevLett.121.086803.
- [26] K. Zhang, Z. Yang, C. Fang, Correspondence between winding numbers and skin modes in non-hermitian systems, *Phys. Rev. Lett.* 125 (2020) 126402. doi:10.1103/PhysRevLett.125.126402.
- [27] X. Zhang, T. Zhang, M.-H. Lu, Y.-F. Chen, A review on non-Hermitian skin effect, *Advances in Physics: X* 7 (1) (2022) 2109431. doi:10.1080/23746149.2022.2109431.
- [28] F. K. Kunst, V. Dwivedi, Non-Hermitian systems and topology: A transfer-matrix perspective, *Phys. Rev. B* 99 (2019) 245116. doi:10.1103/PhysRevB.99.245116.
- [29] K. Yokomizo, S. Murakami, Non-Bloch band theory of non-Hermitian systems, *Phys. Rev. Lett.* 123 (2019) 066404. doi:10.1103/PhysRevLett.123.066404.
- [30] Z. Yang, K. Zhang, C. Fang, J. Hu, Non-Hermitian bulk-boundary correspondence and auxiliary generalized Brillouin zone theory, *Phys. Rev. Lett.* 125 (2020) 226402. doi:10.1103/PhysRevLett.125.226402.
- [31] N. Hatano, D. R. Nelson, Localization transitions in non-Hermitian quantum mechanics, *Phys. Rev. Lett.* 77 (1996) 570–573. doi:10.1103/PhysRevLett.77.570.
- [32] W. P. Su, J. R. Schrieffer, A. J. Heeger, Solitons in polyacetylene, *Phys. Rev. Lett.* 42 (1979) 1698–1701. doi:10.1103/PhysRevLett.42.1698.
- [33] A. Melkani, J. Paulose, Space-time symmetry and parametric resonance in dynamic mechanical systems, arXiv preprint arXiv:2310.08734 (2023).
- [34] A. Ghatak, M. Brandenbourger, J. van Wezel, C. Coulais, Observation of non-Hermitian topology and its bulk–edge correspondence in an active mechanical metamaterial, *Proceedings of the National Academy of Sciences* 117 (47) (2020) 29561–29568. doi:10.1073/pnas.2010580117.

- [35] F. Tisseur, K. Meerbergen, The quadratic eigenvalue problem, SIAM Review 43 (2) (2001) 235–286. doi:10.1137/S0036144500381988.
- [36] A. Mostafazadeh, Pseudo-Hermiticity versus PT symmetry: The necessary condition for the reality of the spectrum of a non-Hermitian Hamiltonian, Journal of Mathematical Physics 43 (1) (2002) 205–214. doi:10.1063/1.1418246.